Terahertz Detection and Imaging Using Graphene Ballistic Rectifiers

Gregory Anton, Dmytro B. But, Jiawei Zhang, Ernie Hill, Dominique Coquillat, Christophe Consejo, Philippe Nouvel, Wojciech Knap, Luca Varani, Frederic Teppe, et al.

NANO LETTERS

Letter

pubs.acs.org/NanoLett

Terahertz Detection and Imaging Using Graphene Ballistic Rectifiers

Gregory Auton,[†,‡] Dmytro B. But,[§] Jiawei Zhang,[†] Ernie Hill,[‡] Dominique Coquillat,[§] Christophe Consejo,[§] Philippe Nouvel,[∥] Wojciech Knap,[§] Luca Varani,[∥] Frederic Teppe,[§] Jeremie Torres,*[,∥] and Aimin Song*[,†,⊥]

[†]School of Electrical and Electronic Engineering and [‡]Manchester Centre for Mesoscience and Nanotechnology, University of Manchester, Manchester M13 9PL, United Kingdom

[§]Laboratoire Charles Coulomb (L2C), Université de Montpellier, CNRS UMR 5221, 34090 Montpellier, France

[∥]Institut d'Electronique et des Systèmes (IES), Université de Montpellier, CNRS UMR 5114, 34090 Montpellier, France

[⊥]Center of Nanoelectronics, State Key Laboratory of Crystal Materials, and School of Microelectronics, Shandong University, Jinan, 250100, China

Supporting Information

ABSTRACT: A graphene ballistic rectifier is used in conjunction with an antenna to demonstrate a rectenna as a terahertz (THz) detector. A small-area (<1 μm^2) local gate is used to adjust the Fermi level in the device to optimize the output while minimizing the impact on the cutoff frequency. The device operates in both n- and p-type transport regimes and shows a peak extrinsic responsivity of 764 V/W and a corresponding noise equivalent power of 34 pW $Hz^{-1/2}$ at room temperature with no indications of a cutoff frequency up to 0.45 THz. The device also demonstrates a linear response for more than 3 orders of magnitude of input power due to its zero threshold voltage, quadratic current−voltage characteristics and high saturation current. Finally, the device is used to take an image of an optically opaque object at 0.685 THz, demonstrating potential in both medical and security imaging applications.

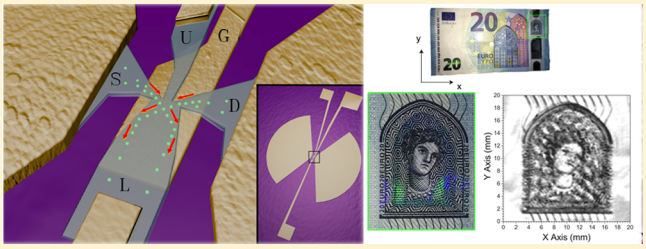

KEYWORDS: *Graphene, rectenna, THz, ballistic transport, rectifier*

Interest in terahertz (THz) detection[1−13] originates from a wide range of applications in the fields of medicine, security, and nondestructive quality testing that are either complementary to or simply cannot be achieved by techniques in other electromagnetic radiation frequency bands. Radiation in the THz frequency region can penetrate common dielectric materials that would otherwise be opaque at optical frequencies. It is also both nonionizing (therefore safer than X-rays) and capable of being used to identify materials spectroscopically.[8] Current THz detection technology requires cryogenic cooling to reach a very high sensitivity, e.g., a typical superconducting bolometer has a noise equivalent power (NEP) in the order of 1 pW $Hz^{-1/2}$ at 8 K (ref 12). Room-temperature devices (such as pyroelectric detectors or Golay cells) are usually limited to an NEP of 10 pW $Hz^{-1/2}$ (ref 4). Both these cryogenic and room-temperature devices suffer from slow response times due to their working principles, hence limiting modulation frequencies to ∼100 Hz (ref 13). An alternative to these detectors is to use an antenna coupled to a high-speed nonlinear electronic component such as a Schottky diode or a field effect transistor (FET). The combination of an antenna with a rectifying element is aptly named the rectenna.[14,15] The functionality of a rectenna is fundamentally limited by the properties of the rectifying element, and most Schottky diodes have a cutoff frequency well below 1 THz unless a challenging nanoscale air-bridge to one of the electrodes can be fabricated in order to reduce the parasitic capacitance.[13,16] Furthermore, due to the exponential current−voltage characteristics of Schottky diode, the input dynamic range in which the diode shows a linear input-power dependence or quadratic behavior is often quite limited. Terahertz detectors based on plasma wave resonances in field-effect transistors (FETs) have also been demonstrated recently. One such Si FET THz detector demonstrated a wide operational range between 0.25 and 1.04 THz and a minimum NEP of 10 pW $Hz^{-1/2}$ (ref 7). However, this example uses the antenna footprint rather than the diffraction limit as the effective area of the detector making it difficult to directly compare this value to standard detectors.

With the highest room-temperature carrier mobility, a high current flux, and a high saturation velocity, graphene is an excellent candidate for high-frequency electronics.[3,5,11] However, without a bandgap it has proven difficult to use graphene in transistor technologies because the resulting devices had low on/off ratios.[17,18] Various methods have been used to create a bandgap such as reducing the graphene channel width to create a graphene nanoribbon (GNR).[19] Unfortunately, edge defects

Received: August 23, 2017
Revised: October 9, 2017
Published: October 10, 2017

DOI: 10.1021/acs.nanolett.7b03625
Nano Lett. 2017, 17, 7015−7020

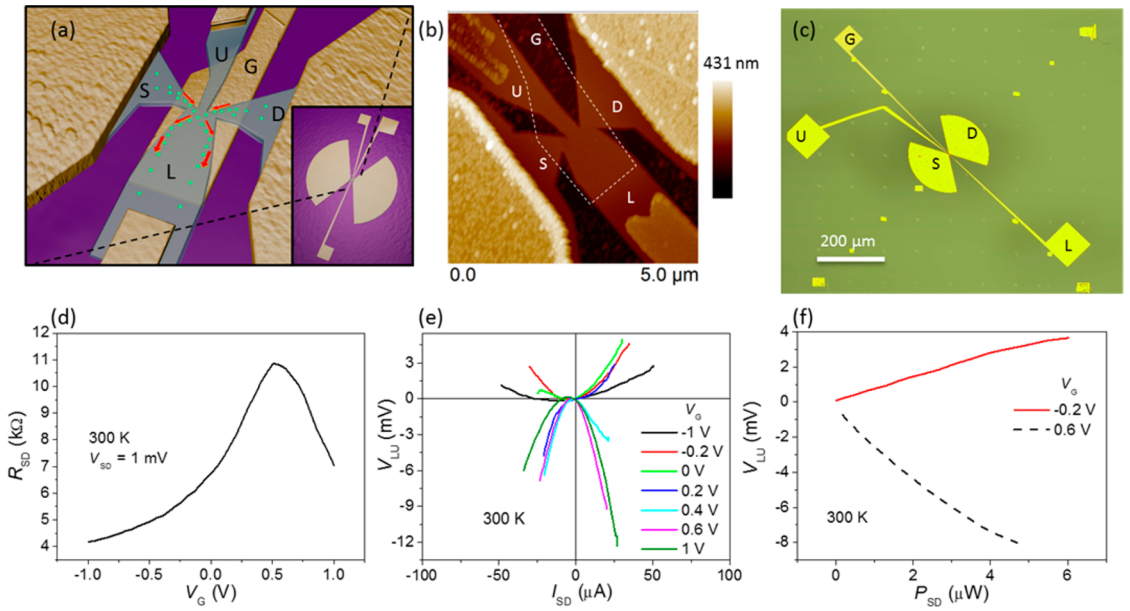

Figure 1. Graphene ballistic rectifier geometry, antenna structure, and dc characterization. (a) A schematic showing the central active region of the ballistic rectifier where the arrows indicate typical carrier trajectories; the inset shows the whole rectenna and the two input contacts connected to the antenna lobes have been labeled source (S) and drain (D) along with the gate (G), lower (L), and upper (U) contacts. (b) An atomic-force micrograph showing the active region of the device with the GBR at its center where the same contacts have been labeled and a dotted line has been drawn around the edge of the localized gate as a guide for the eye. (c) A 10× optical image of the device where the same contacts have been labeled. (d) dc measurement of R_{SD} against V_G while 1 mV was applied to V_{SD}. (e) dc measurements of V_{LU} against I_{SD} at different gate voltages. (f) dc measurement of V_{LU} against P_{SD} at the peak output for holes and electrons.

usually dominate the transport properties of the GNR and the mobility is heavily impacted. The graphene tunnelling transistor has a high on/off ratio but by its very nature has a high capacitance and therefore it would be highly challenging to achieve a high operating speed.[20] Graphene FET THz detectors have been demonstrated with an NEP of 515 pW $Hz^{-1/2}$ at 0.6 THz;[21] other such examples have been less sensitive.[5,11,22,23] The photothermoelectric effect in graphene has been used to produce an NEP of 1.1 nW $Hz^{-1/2}$ at 1.02 THz.[24]

Unlike transistors that depend on the bandgap, certain diodes are able to take the advantage of the very high carrier mobility of graphene but are less limited by the absence of a bandgap. One such device is called the ballistic rectifier (BR), which is an asymmetric four-terminal cross-junction that relies on the ballistic motion of carriers to rectify alternating currents (ac) signals into direct currents (dc) outputs.[25] In the ballistic regime of electron transport, carriers have a mean free path longer than the characteristic dimension of the device, meaning that uncontrolled and random scatterings off phonons or impurities can be neglected. Instead, they scatter off the designed edges of the device so that they are redirected to predetermined directions like billiard balls. The BR was first demonstrated in InGaAs/AlGaAs heterostructures and its full-wave rectifying functionality resembles that of a bridge rectifier, which in contrast requires four individual diodes. As shown by the typical carrier trajectories in Figure 1a and Supporting Information, the carriers are redirected to the same output lead irrespective of which input contact they come from, resulting in a dc output when an ac signal is applied. The four-terminal nature of the device and the orthogonal arrangement of the input channels to the output channels ensure that the input and output contacts are largely decoupled, and the output noise is slightly influenced by the input signal.[26] The BR concept inherently differs from all conventional rectifiers because it neither contains nor relies on any doping junction or barrier structure along the direction of electrical current. As such, the carriers do not need to overcome a built-in electric field to conduct a current, meaning that the device has a zero threshold voltage.[27] This is an advantage because, otherwise, the detector would have to be biased which introduces noise in the output and also additional parasitic capacitance that affects the cutoff frequency.[8] Finally, unlike conventional diodes or transistors, the new working principle does not require a material with an energy bandgap and the device speed scales up with the carrier mobility. Hence, graphene, despite having a zero bandgap, is ideal for the fabrication of BRs.

Recently, we reported the high sensitivity of graphene ballistic rectifiers (GBR) at low frequency.[28] However, these devices were fabricated with a global back gate and therefore could only be tested at frequencies up to 3 MHz. Earlier devices based on a conventional semiconductor InGaAs were measured up to 50 GHz.[29] With a mobility up to 20 times higher than that in InGaAs, the graphene BR is expected to function well into the high THz frequency range, since the speed generally scales linearly with the carrier mobility. Furthermore, at THz frequencies antenna-rectifier impedance mismatch becomes crucial and may significantly affect the extrinsic properties. Here, we fabricate a small-area local gate and integrate the ballistic rectifier with a broadband antenna, which enables us to characterize the high-frequency response and demonstrate THz imaging at frequencies up to 0.685 THz.

Figure 1a shows a schematic of the central active region of the ballistic rectifier where the arrows indicate typical carrier trajectories. The inset shows the whole rectenna. The two input contacts connected to the antenna lobes have been labeled source (S) and drain (D) along with gate (G), lower (L), and upper (U) contacts. The graphene flake is encapsulated between two boron nitride (BN) flakes with thicknesses

DOI: 10.1021/acs.nanolett.7b03625
Nano Lett. 2017, 17, 7015−7020

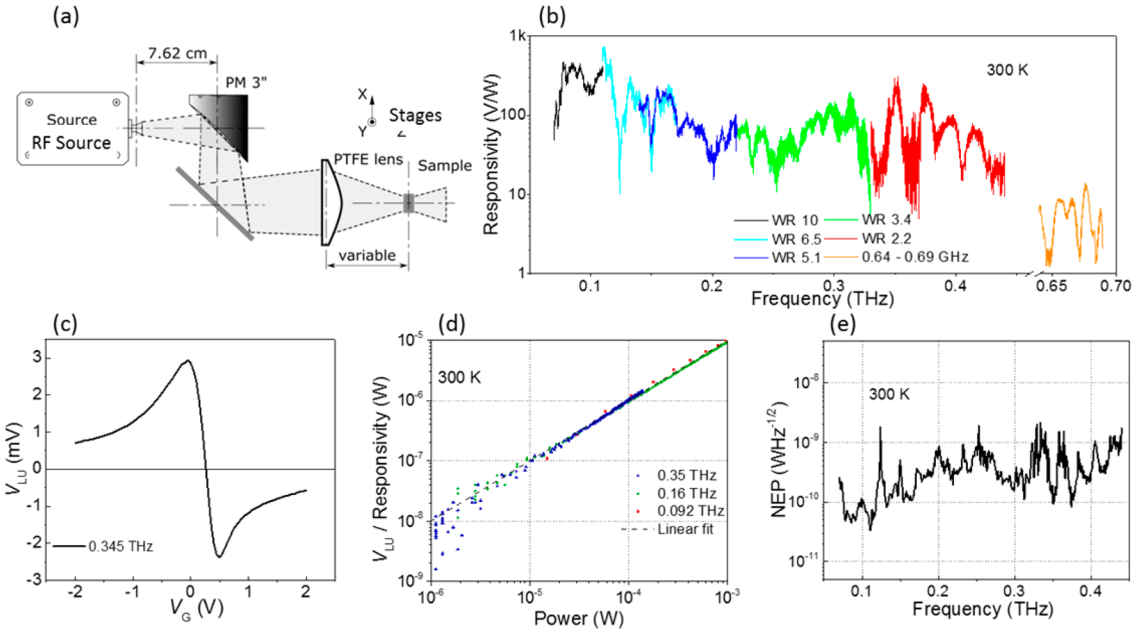

Figure 2. THz characterization of a graphene ballistic rectenna. (a) A schematic of the setup used for the free-space measurements. (b) Extrinsic responsivity of the device across the frequency spectrum which was calculated by assuming the effective area of the device to be $\frac{\lambda^2}{4\pi}$. (c) V_{LU} versus V_G while 0.345 THz was applied to the device. (d) $\frac{V_{LU}}{\mathcal{R}}$ of the device versus incident power on the device at different frequencies showing a wide range of linear power dependence. (e) NEP against frequency.

varying from device to device but in this case both flakes were ∼40 nm measured by optical contrast. Figure 1b is an atomic force micrograph (AFM) showing the active region of the device with the GBR at its center (Supporting Information shows a scanning-electron micrograph of the same device). A dotted line has been drawn around the edge of the localized gate as a guide for the eye. The bottom BN layer was used as the gate dielectric. The narrow injection channels (S and D) were measured to be 356 and 335 nm at the narrowest part, slightly different due to imperfection in fabrication. The gate thickness was minimized to 3/20 nm (Cr/Au) to allow the flake stack on all sides to relax back onto the substrate before it meets the contacts and antenna lobes. Figure 1c is a 10× optical image of the device where the same contacts have been labeled for clarity.

The GBR was fabricated using mechanically exfoliated graphene and BN flakes. First, a quartz substrate was prepared with Cr/Au (3/20 nm) crosses and local back gate contact. A BN/graphene/BN stack was then prepared by stamp transfer as described in ref 28; the strain from bending the flake stack over the local gate ensures there was no contamination bubble between the flakes on the gated region. The antenna and contacts were then defined using electron beam lithography (EBL), after which the stack is etched and the sample metalized with Cr/Au (3/70 nm) to make one-dimensional contacts as described in ref 28. A PMMA etch mask was then defined to protect the desired areas of graphene and BN for the device during the following etch. Finally, the antenna was thickened to 250 nm by further metal deposition using EBL to increase the absorption of THz.

In order to understand features observed when the antenna is used to receive a THz signal to couple to the device, it is important to investigate the dc properties of the device. This was achieved using a probe station to avoid damaging the antenna. Figure 1d is a dc measurement of the resistance between S and D (R_{SD}) against gate voltage (V_G) while 1 mV was applied between S and D (V_{SD}) showing that the charge neutrality point (CNP) of the bulk graphene was 0.5 V. It is also observed that the local gate can effectively tune the Fermi level even at relatively low gate voltages (less than 1 V). The high impedance of the device, R_{SD} of 6768 Ω at zero gate bias, implies a large impedance miss-match to the antenna (R_A ∼ 100 Ω).

Figure 1e shows dc measurements of the voltage between L and U (V_{LU}) against the current between S and D (I_{SD}) at different gate voltages. With both positive and negative quadratic output, the device is behaving as expected for holes and electrons, respectively. Again, the curves are not perfectly symmetric through the vertical axis due to imperfections in nanofabrication.

According to a quantitative model in ref 27, which was on a slightly different design, the rectifying functionality is based on the collimating effect of carriers induced by the applied current. The collimating effect changes the carrier transmission probabilities from S and D to the L and U terminals, and hence according to the Büttiker−Landauer formalism induces a dc voltage difference between L and U. For a low input signal, the quadratic dependence of the output on the input can be expressed by

$$V_{LU} \propto \frac{1}{E_F N_{SD}(N_{LU} - N_{SD})} I_{SD}^2 \quad (1)$$

where E_F is the Fermi energy, N_{SD} is the number of occupied transverse confinement modes in the S and D channels, and N_{LU} is the number of occupied transverse confinement modes in the L and U channels.[30] As eq 1 suggests, the GBR operates optimally at low carrier densities, which corresponds to a low Fermi energy and hence fewer occupied lateral conduction modes. However, when it is too close to the CNP in graphene,

DOI: 10.1021/acs.nanolett.7b03625
Nano Lett. 2017, 17, 7015−7020

the coexistence of both carrier types due to thermal excitation leads to a reduction of the output.[28] Since V_G was set relative to the grounded source, V_{SD} will effect the relative potential of the gate by $V_{SD}/2$. Close to the CNP it is possible to change the type of dominant carrier with V_{SD} and observe both positive and negative output from the same gate voltage. The result is that when V_G = 0.2 V the positive (negative) bias displays positive (negative) curvature because $V_G < V_{SD}/2$ ($V_G > V_{SD}/2$) and holes (electrons) are the dominant carrier. Figure 1f is a dc measurement of V_{LU} against the dc power applied between S and D (P_{SD}) at the peak output for holes and electrons. From this, the intrinsic responsivity of the device can be estimated to be 3200 and 850 V/W for electrons and holes, respectively. While these sensitivities are high they are not as impressive as previous examples of GBRs[28,31] because these two point measurements include power lost as a result of the contact resistance. Also, the device size was increased to achieve a lower resistance and therefore better impedance matching to the antenna. A larger ballistic device will have a longer path length meaning that statistically more carriers will scatter diffusively and therefore will be less efficient.

Figure 2a shows a schematic of the setup used for the free-space measurements. To highlight the ability of these devices to detect THz radiation, we have used electronic sources from Virginia Diodes Inc. (VDI) to cover a large frequency range from 0.07 to 0.69 THz in bands but with an overlap between each band. As this kind of electronic source is composed of a multiplication chain, the measurement frequency points have been verified to be spurious free (e.g., monochromatic signal). The radiation power was measured by a calibrated pyroelectric detector[32] at the device position. The THz signal was modulated around 600 Hz. Regarding the optical path, the beam was collimated using a gold-coated parabolic mirror of 152.4 mm effective focal length then focused by a specially designed Teflon (PTFE) lens. The distance between this lens and the device was adapted for the frequency range. The incoming THz radiation has linear polarization with a Gaussian intensity distribution and was incident normal to the surface of the sample. The device was mounted on a DIP-holder. The induced device output is measured using standard lock-in/mechanical chopper detection scheme between L and U contacts. The motorized linear stages provided precise positioning of the detector.

Figure 2b is a plot showing the extrinsic responsivity ($\mathcal{R}$) of the device across the frequency spectrum, given by the dc output V_{LU} divided by the incident power on the device. The total output power of the THz source was measured by a pyroelectric detector (see Supporting Information) and the spot size of the radiation was measured independently (an example can be seen in Supporting Information). There is very little agreement in the literature with regards to how to estimate the power received by the antenna when determining the responsivity. One of the common methods is to use the physical surface area of the antenna, which will typically give the largest values of responsivity.[6] Alternatively, the total power in the beam spot produced by a particular measurement setup is often used, which typically gives the lowest values of responsivity.[21] In this work, the effective area of the antenna was taken to be $\frac{\lambda^2}{4\pi}$ where λ is the wavelength of the radiation.[33,34] This also has the advantage of being able to take into account the frequency dependence that the other two methods are incapable of. The thus obtained value of $\mathcal{R}$ up to 764 V/W is, to our knowledge, the highest reported for a graphene-based room-temperature device for THz detection.[5,11,21−23]

A finite element simulation performed using the software package CST-microwaves reveals that the antenna has the best reception between 0.29 and 0.42 THz (Supporting Information) and indeed the experimental data in Figure 2b shows a good agreement. The repeatability of the measurements was excellent, which can be seen clearly when the outputs from the different THz sources overlapped (one example is shown in Supporting Information). The devices with encapsulation showed stability over the many months that the experiments in this work took place with little change in the current−voltage characteristics.

Figure 2c shows V_{LU} as a function of V_G while 0.345 THz radiation was applied to the device. A number of devices have been fabricated and they all showed similar behavior. Supporting Information shows two of the devices. However, in Figure 2c the holes show a superior output when compared to the electrons, while Figure 1e,f shows electrons with a superior output. This could be because the intrinsic majority carrier in the graphene is holes and only the very central region of the device has a backgate resulting in n−p structures forming at the edges of the gate. These structures could result in higher impedance values while electrons are majority carriers in the gated region[35,36] and therefore would result in worse impendence matching.

Figure 2d is a graph showing $\frac{V_{LU}}{\mathcal{R}}$ of the device against THz power incident on the device at different frequencies showing linear behavior that is expected from the quadratic dependence shown in eq 1.[28] While the exponential dependency observed in most diode devices may be preferable when input signals are large, THz signals are normally very small and for this reason quadratic behavior is preferable. In this figure, the voltage output has been divided by the responsivity to remove any frequency dependency from the antenna and show the flat frequency response from the GBR. The device demonstrates excellent linear voltage response over 3 orders of magnitude of power input measured due to its zero threshold and high saturation current. Good linearity and wide dynamic range are desirable features of microwave and THz detectors.

One of the most important figures of merit for a detector is the noise equivalent power (NEP), which describes the lowest power detectable with a one-Hz bandwidth. The value of the NEP can be calculated by dividing the noise by the $\mathcal{R}$. In the case of a normal two-terminal diode, the nonlinearity in the current−voltage characteristics is usually on top of a large dc bias component, and the dominant low-frequency flicker noise (also called $1/f$ noise) is proportional to the bias current. In the ballistic rectifier, however, such an issue is eliminated since the output channels U and L are placed in the perpendicular direction or orthogonal to the input current between S and D, and the output consists of only the net rectified signal. Furthermore, the BR has an intrinsic zero threshold, which further eliminates flicker noise in the device.[27] Figure 2e is a graph showing NEP against frequency using the interpolated sensitivity results from Figure 2a and calculating NEP from

$$NEP = \frac{\sqrt{4kTR_{LU}}}{\mathcal{R}}$$

where T is 300 K and R_{LU} is the resistance between L and U and was taken to be 25 kΩ (see Supporting Information). The

DOI: 10.1021/acs.nanolett.7b03625
Nano Lett. 2017, 17, 7015−7020

minimum of NEP was then found to be 34 pW $Hz^{-1/2}$, over an order of magnitude better than examples of graphene field-effect devices.[5,11,21−23]

Figure 3 shows the normalized voltage signal from the device as a function of the polarization angle of the input THz wave.

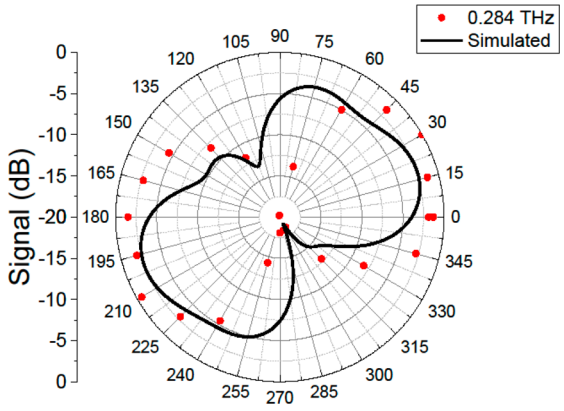

Figure 3. Polarization dependence: a comparison between data and simulation. Normalized voltage signal from the device as a function of the polarization angle of the input THz wave shown by the red dots. The black line is a plot of simulated gain against angular response from the antenna modeled using the finite element software CST-Microwaves.

The black line shows a plot of simulated gain against angular response from the antenna modeled using the finite element software CST-Microwaves that compares well withFigure 3. The frequency was chosen because it represented the peak in V_{LU} output. The asymmetry is due to the layout of the localized gate and contact.

Figure 4a is a schematic of a THz imaging setup featuring two focal points, one for the sample to be raster scanned through and the other for the rectifying device to measure the transmitted power. A frequency chain multiplied THz source from Virginia Diodes Inc.[37] at 0.685 THz was used as a THz source. The THz radiation was focused by a system of mirrors (flat and parabolic) and a PTFE lens before being collimated and focused on the detector by another system of mirrors and lenses. The detector signal was registered using a lock-in system that was synchronized with the modulation of the THz source. The image of the bank note was obtained by moving it with linear stages in front of the THz beam.

Figure 4b is an optical image of a €20 bank note and Figure 4c is a magnified optical image of a region of the security feature on the note. The THz image of the security feature region in Figure 4d was achieved by plotting the output signal from the GBR while the note was raster scanned through a second focal point with a THz beam fixed at 0.685 THz. The scan was achieved at a speed of 10 ms/pixel with a resolution of 666 × 800 and a spot size of ∼500 μm (see Supporting Information Figure 8). In practice, multiplexing of many devices on a chip would be used instead of raster scanning a single device to generate an image for a commercial application. This device is both highly sensitive and operates at room temperature making it ideal for security or medical THz imaging applications. The end product would be both portable and cheap due to its on-chip design and simple fabrication procedures enabled by the single-layered planar device architecture and straightforward integration with an antenna without the need to fabricate nanoscale air bridges. The sensor could be further improved by adding a silicon lens on the backside to avoid THz modes within the substrate and help focus from the rear facet of the chip onto the device, providing better coupling with modes in the antenna. A waveguide and integrated amplifier would also allow for greater signal output. The ballistic rectifier might be improved by matching the antenna impedance more closely; this could be achieved by using bilayer graphene or multiple layers of graphene separated by thin BN spacers allowing several devices to be in parallel across one antenna.

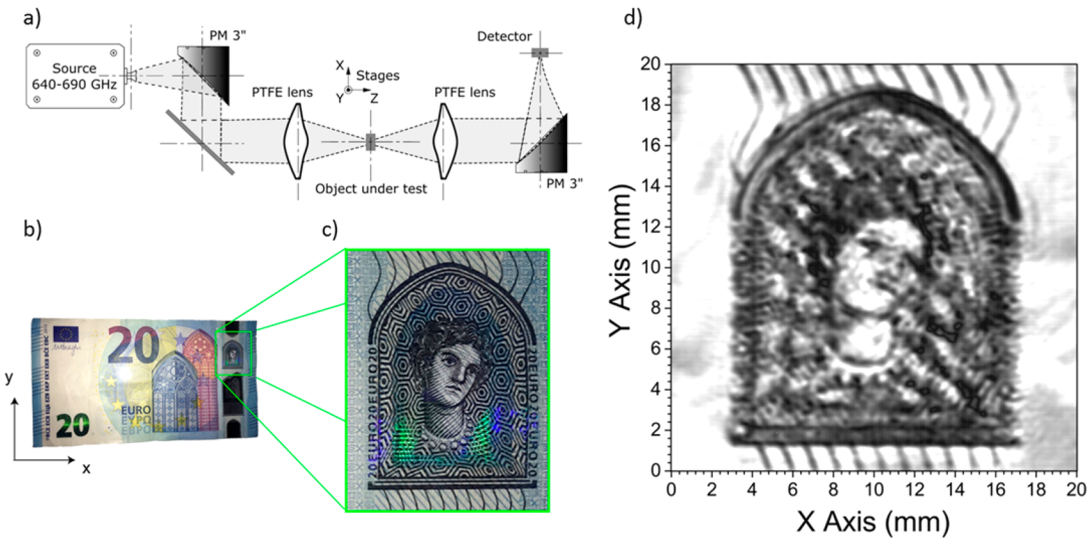

Figure 4. THz imaging. (a) A schematic of a THz imaging setup featuring two focal points, one for the sample to be raster scanned through and the other for the rectifying device to measure the transmitted power. (b) An optical image of a € 20 bank note. (c) A zoomed optical image of a region of the security feature on the note. (d) The THz image of the security feature region, achieved by plotting the signal from the device while the note was raster scanned through a second focal point in the THz beam fixed at 0.685 THz.

DOI: 10.1021/acs.nanolett.7b03625
Nano Lett. 2017, 17, 7015−7020

■ ASSOCIATED CONTENT

Supporting Information

The Supporting Information is available free of charge on the ACS Publications website at DOI: 10.1021/acs.nanolett.7b03625.

Details of device structure, radio frequency characterization, and measurement calibration (PDF)

■ AUTHOR INFORMATION

Corresponding Authors

*E-mail: jeremie.torres@umontpellier.fr.
*E-mail: A.Song@manchester.ac.uk.

ORCID

Aimin Song: 0000-0001-6550-518X

Author Contributions

G.A. and J.Z. fabricated the devices and performed DC measurements. D.B., D.C., and C.C. performed high-frequency measurements. P.N. and W.K. performed electromagnetic simulations. A.S., J.T., L.V., F.T., and E.H. conceived and designed the experiments.

Notes

The authors declare no competing financial interest.

■ ACKNOWLEDGMENTS

This work has been supported by the National Key R&D Program of China (2016YFA0301200), National Natural Science Foundation of China (11374185), Engineering and Physical Sciences Research Council (EP/M507969/1, EP/G03737X/1, EP/N021258/1), the Agence nationale de la Recherche project Integrated Nano-Detectors for terahertz Applications (ANR-13-NANO-0008), the Terahertz Platform TOP and by the Occitanie region via the Gepeto Terahertz platform, and by Eranet-Rus-Plus European program Terasens.

■ REFERENCES

(1) Ferguson, B.; Zhang, X. C. Materials for terahertz science and technology. *Nat. Mater.* **2002**, *1*, 26−33.
(2) Gadalla, M. N.; Abdel-Rahman, M.; Shamim, A. Design, optimization and fabrication of a 28.3 THz nano-rectenna for infrared detection and rectification. *Sci. Rep.* **2015**, *4*, 4270.
(3) Zhu, Z.; Joshi, S.; Grover, S.; Moddel, G. Graphene geometric diodes for terahertz rectennas. *J. Phys. D: Appl. Phys.* **2013**, *46*, 185101.
(4) Lee, M.; Wanke, M. C. Searching for a solid-state terahertz technology. *Science* **2007**, *316*, 64−65.
(5) Vicarelli, L.; et al. Graphene field-effect transistors as room-temperature terahertz detectors. *Nat. Mater.* **2012**, *11*, 865−871.
(6) Ahmad, Z.; Lisauskas, A.; Roskos, H. G.; Kenneth, K. O. 9.74-THz electronic Far-Infrared detection using Schottky barrier diodes in CMOS. *IEEE Int. Elec. Dev. Meeting.* **2014**, 4.4.1.
(7) Schuster, F.; et al. Broadband terahertz imaging with highly sensitive silicon CMOS detectors. *Opt. Express* **2011**, *19*, 7827−7832.
(8) Tonouchi, M. Cutting-edge terahertz technology. *Nat. Photonics* **2007**, *1*, 97−105.
(9) El Fatimy, A.; et al. Epitaxial graphene quantum dots for high-performance terahertz bolometers. *Nat. Nanotechnol.* **2016**, *11*, 335−338.
(10) Williams, B. S. Terahertz quantum-cascade lasers. *Nat. Photonics* **2007**, *1*, 517−525.
(11) Bianco, F.; et al. Terahertz detection by epitaxial-graphene field-effect-transistors on silicon carbide. *Appl. Phys. Lett.* **2015**, *107*, 131104.
(12) Mittleman, D. *Sensing with Terahertz Radiation*; Springer-Verlag: Berlin, 2003.
(13) Sizov, F.; Rogalski, A. THz detectors. *Prog. Quantum Electron.* **2010**, *34*, 278−347.
(14) Donchev, E.; et al. The rectenna device: From theory to practice (a review). *MRS Energy & Sustainability* **2014**, *1*, 1−34.
(15) McSpadden, J. O.; Fan, L.; Chang, K. Design and experiments of a high-conversion-efficiency 5.8-GHz rectenna. *IEEE Trans. Microwave Theory Tech.* **1998**, *46*, 2053−2060.
(16) Ito, H.; Muramoto, Y.; Yamamoto, H.; Ishibashi, T. Matching-Circuit-Integrated InGaAsP Schottky Barrier Diode for Zero-Biased Operation in the Sub-Millimeter-Wave Range. *Jpn. J. of Appl. Phys.* **2012**, *51*, 114101.
(17) Novoselov, K. S.; et al. Electric field effect in atomically thin carbon films. *Science* **2004**, *306*, 666−669.
(18) Novoselov, K. S.; et al. Two-dimensional gas of massless Dirac fermions in graphene. *Nature* **2005**, *438*, 197−200.
(19) Han, M. Y.; Özyilmaz, B.; Zhang, Y.; Kim, P. Energy Band-Gap Engineering of Graphene Nanoribbons. *Phys. Rev. Lett.* **2007**, *98*, 206805.
(20) Britnell, L.; et al. Field-Effect Tunneling Transistor Based on Vertical Graphene Heterostructures. *Science* **2012**, *335*, 947−950.
(21) Zak, A.; et al. Antenna-integrated 0.6 THz FET direct detectors based on CVD graphene. *Nano Lett.* **2014**, *14*, 5834−5838.
(22) Spirito, D.; et al. High performance bilayer-graphene terahertz detectors. *Appl. Phys. Lett.* **2014**, *104*, 061111.
(23) Tong, J.; et al. Antenna enhanced graphene THz emitter and detector. *Nano Lett.* **2015**, *15*, 5295−5301.
(24) Cai, X.; et al. Sensitive room-temperature terahertz detection via the photothermoelectric effect in graphene. *Nat. Nanotechnol.* **2014**, *9*, 814−819.
(25) Song, A. M.; et al. Nonlinear electron transport in an asymmetric microjunction: a ballistic rectifier. *Phys. Rev. Lett.* **1998**, *80*, 3831.
(26) Singh, A. K.; Kasjoo, S. R.; Song, A. M. Low-Frequency Noise of a Ballistic Rectifier. *IEEE Trans. Nanotechnol.* **2014**, *13*, 527−531.
(27) Song, A. M. Formalism of nonlinear transport in mesoscopic conductors. *Phys. Rev. B: Condens. Matter Mater. Phys.* **1999**, *59*, 9806−9809.
(28) Auton, G.; et al. Graphene ballistic nano-rectifier with very high responsivity. *Nat. Commun.* **2016**, *7*, 11670.
(29) Song, A. M.; et al. Operation of InGaAs/InP-based ballistic rectifiers at room temperature and frequencies up to 50 GHz. *Jpn. J. Appl. Phys.* **2001**, *40*, L909.
(30) Song, A. M. Electron ratchet effect in semiconductor devices and artificial materials with broken centrosymmetry. *Appl. Phys. A: Mater. Sci. Process.* **2002**, *75*, 229−235.
(31) Auton, G.; Kumar, R. K.; Hill, E.; Song, A. Graphene Triangular Ballistic Rectifier: Fabrication and Characterisation. *J. Electron. Mater.* **2017**, *46*, 3942.
(32) Müller, R.; et al. Novel detectors for traceable THz power measurements. *J. Infrared, Millimeter, Terahertz Waves* **2014**, *35*, 659−670.
(33) Sakhno, M.; Golenkov, A.; Sizov, F. Uncooled detector challenges: Millimeter-wave and terahertz long channel field effect transistor and Schottky barrier diode detectors. *J. Appl. Phys.* **2013**, *114*, 164503.
(34) But, D. B.; et al. Nonlinear photoresponse of field effect transistors terahertz detectors at high irradiation intensities. *J. Appl. Phys.* **2014**, *115*, 164514.
(35) Williams, J. R.; DiCarlo, L.; Marcus, C. M. Quantum Hall effect in a gate-controlled p−n junction of graphene. *Science* **2007**, *317*, 638−641.
(36) Gorbachev, R. V.; et al. Conductance of p-n-p graphene structures with "air-bridge" top gates. *Nano Lett.* **2008**, *8*, 1995−1999.
(37) Crowe, T. W.; Bishop, W. L.; Porterfield, D. W.; Hesler, J. L.; Weikle, R. M. Opening the terahertz window with integrated diode circuits. *IEEE J. Solid-State Circuits* **2005**, *40*, 2104−2110.

DOI: 10.1021/acs.nanolett.7b03625
Nano Lett. 2017, 17, 7015−7020